Eur. J. Mech. B/Fluids, **17**, n° 3, 307-329, 1998

A contribution to the physical analysis of separated flows past three-dimensional humps

C. ROGET [ab], J. Ph. BRAZIER [a]*, J. COUSTEIX [a] and J. MAUSS [b]

ABSTRACT. – The aim of this article is to present a few improvements in the understanding of both mathematical and physical aspects of three-dimensional separated flows past a protuberance on a flat plate. Only steady laminar incompressible flows are considered here. The asymptotic structure of boundary-layer flows with strong viscous-inviscid interaction has been extensively studied by several authors, mainly with the triple-deck theory. The first part of this paper presents the results of a systematic analysis of the asymptotic structure when the obstacle's dimensions vary. This work explains why the triple-deck properties are so much characteristic. The three-dimensional boundary-layer equations are then solved with a quasi-simultaneous interacting technique, and the results are examined in order to describe the three-dimensional topology of the flow. Two types of flows are described, corresponding to a dent and a hump, that exhibit completely different behaviours. © Elsevier, Paris

1. Introduction

The problem of laminar boundary-layer separation past an obstacle has been investigated by many authors for several decades. The theoretical bases rely on the famous *Triple-Deck* theory (Stewartson, 1969), which made it possible to solve the problem of the Goldstein singularity at separation. Following this breakthrough, many works, mainly from F.T. Smith, were dedicated to the application of the triple-deck theory to separated flows past small two-dimensional humps (for example Smith, 1973, 1981) then three-dimensional ones (Smith *et al.*, 1977, 1980, Sykes, 1980, Bogolepov and Lipatov, 1985), also providing the first numerical solutions. This theory was also found valuable for internal flows (for example Smith, 1976a, 1976b, 1980) even if the flow behaviour near separation is not exactly the same for a pipe flow and for an external boundary layer.

The key feature of the triple-deck theory is the strong interaction between the boundary layer and the inviscid flow. Adding this interaction to the ordinary boundary-layer equations constitutes the Interacting Boundary Layer theory (IBL), which has been used extensively by many authors for two-dimensional flows, giving nice results in good accordance with the triple-deck asymptotic solutions. Some critical reviews and numerous references can be found in articles by Ragab and Nayfeh (1981), McDonald and Briley (1983), Smith (1986), Henkes and Veldman (1987), Rothmayer and Barnett (1991).

From a numerical point of view, the first IBL methods solved the boundary-layer equations in either direct or inverse mode, and the inviscid flow separately. This procedure resulted in low efficiency and instabilities when switching between direct and inverse modes. A significant improvement was obtained by Veldman (1979, 1981) with a new numerical algorithm in which the boundary-layer equations and the subsonic interaction law are solved simultaneously. It is then no longer necessary to choose either the direct or inverse mode, since

[a] Département d'Études et de Recherches en Aérothermodynamique, ONERA-CERT, 2 avenue Edouard Belin, B.P. 4025, 31055 Toulouse Cedex 4, France

[b] Institut de Mécanique des Fluides de Toulouse UMR-CNRS, Université Paul Sabatier, 118 route de Narbonne, 31062 Toulouse Cedex, France

* Correspondence and reprints

0997-7546/98/03/© Elsevier, Paris

both are included in this procedure. The ellipticity of the Cauchy integral representing the inviscid flow at the wall is thereby better taken into account.

Concerning the three-dimensional flows, some serious difficulties were encountered, due to the ellipticity of the pressure equation, and the appearance of exponential departure solutions when the boundary layer equations are solved by step marching. To solve the non-linear triple-deck equations, Smith (1983) proposed a "skewed shears" formulation, whereas Duck and Burggraf (1986) used a spectral method, solving the Fourier-transform of the equations. Edwards *et al.* (1987) tested several inverse methods for the three-dimensional boundary-layer equations, and Edwards (1987) extended Veldman's simultaneous method to three-dimensional interacting boundary layers past indented flat plates. He could evaluate the influence of the Reynolds number on such flows. His results were successfully compared with Navier-Stokes solutions (Davis *et al.*, 1989). Smith (1991), always with the skewed shears formulation, also obtained numerical solutions for a separated flow past a three-dimensional obstacle with steady interacting boundary-layer equations, and even for the unsteady triple-deck problem. From a different point of view, Le Balleur and Girodroux-Lavigne (1992) computed unsteady three-dimensional separated flows using an integral boundary-layer formulation and a semi-inverse coupling algorithm.

The first part of this paper presents a systematic analysis of the asymptotic structure of the flow past a short-scaled three-dimensional hump, depending on the hump's dimensions. This is similar to the investigation of Smith *et al.* (1981) for two-dimensional obstacles. This systematic approach makes it possible to understand the mechanisms of the triple-deck interaction better. Only the main conclusions will be presented here. A full discussion can be found in Roget (1996).

In the second part, numerical solutions are computed using the interacting boundary-layer theory. The boundary-layer equations and the Cauchy integrals are discretized together and solved simultaneously, using integral thicknesses and pseudo-stream functions, similarly to Edwards' method (Edwards, 1987). Then the results for two types of three-dimensional separated flows, past a dent or a hump, are compared and analyzed, in order to describe the flow behaviour.

2. Asymptotic analysis

2.1. General definitions

We consider a steady incompressible laminar flow past a semi-infinite flat plate. The initial two-dimensional boundary layer encounters a three-dimensional hump which could lead to separation. This hump is located at a distance L_0 from the leading edge. The definition sketch of the three-dimensional flow is given in Figure 1. The Navier-Stokes equations are made dimensionless with U_∞, L_0, and ρU_∞^2 for respectively the velocities, the lengths and the pressure. The x'-direction is parallel to the oncoming flow, the y'-coordinate is normal to the plate, and z' is perpendicular to the former two, such that (x',z',y') is direct. The velocity components are $(u',\ w',\ v')$, and p is the pressure. The Reynolds number is defined as :

$$\mathrm{Re} = \frac{U_\infty L_0}{\nu}$$

The asymptotic parameter ε is then introduced :

$$\varepsilon = \mathrm{Re}^{-1/m} \qquad m > 0 \qquad \varepsilon \ll 1$$

where m is arbitrary. The hump's dimensions are also referred to ε : $lx = \varepsilon^{\alpha}$ is the asymptotic length scale in the x'-direction, whereas $lz = \varepsilon^{\gamma}$ is the asymptotic length scale in the z'-direction and $h = \varepsilon^{\beta}$ is the asymptotic

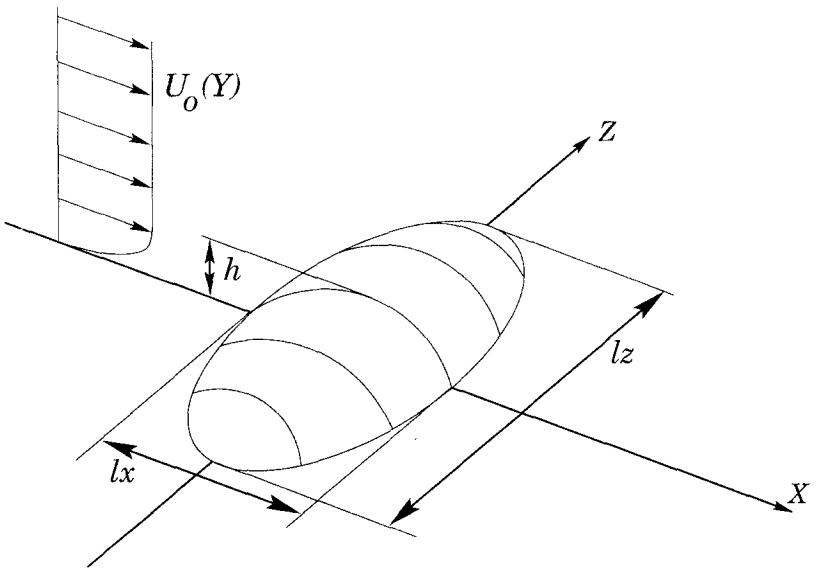

Fig. 1. – Three-dimensional problem.

height scale. The wall perturbation shape is thus given as :

$$y' = \mathcal{F}(x', z') = \varepsilon^{\beta} f\left(\frac{x'}{\varepsilon^{\alpha}}, \frac{z'}{\varepsilon^{\gamma}}\right)$$

where f is of order unity. On the usual way, a Prandtl shift is applied by changing the variables :

$$x = x' \qquad z = z' \qquad y = y' - \varepsilon^{\beta} f(x'/\varepsilon^{\alpha}, z'/\varepsilon^{\gamma})$$

The hump's equation is now just $y = 0$. In order to keep the continuity equation unchanged, the following velocity components are introduced :

$$u = u' \qquad w = w' \qquad v = v' - \varepsilon^{\beta-\alpha} \frac{\partial f}{\partial x} u' - \varepsilon^{\beta-\gamma} \frac{\partial f}{\partial z} w'$$

Three conditions are imposed :

$$\beta > \frac{m}{2} \qquad \beta > \alpha \qquad \beta > \gamma$$

Physically, this means that the protuberance height is less than the incident boundary layer thickness ($\mathrm{Re}^{-1/2} = \varepsilon^{m/2}$), and less than its dimensions in the x and z directions.

2.2. Boundary layer perturbation

We now study the local structure of the flow in the vicinity of the perturbation. We define the new coordinates in the x and z directions as :

$$X = \frac{x}{\varepsilon^{\alpha}} \qquad Z = \frac{z}{\varepsilon^{\gamma}} \qquad Y = \frac{y}{\varepsilon^{m/2}}$$

The (X, Z, Y) coordinates are supposed to be of order unity. The Blasius solution U_b can then be approximated using a Taylor expansion around $x \simeq 0$:

$$U_b(x \simeq 0, Y) = U_0(Y) + O(\varepsilon^{\alpha})$$

where $U_0(Y) = U_b(0, Y)$. The boundary layer perturbations are sought in the general form

$$u = U_0(Y) + \mu \overline{U}(X, Z, Y) \qquad \mu \ll 1$$

where the gauge μ is unknown *a priori*. The Blasius solution is thus supposed to remain the first-order term of the expansion, except in the vicinity of the wall.

A viscous sub-layer must be introduced to satisfy the no-slip condition at the wall, and another upper layer to match the external inviscid flow, giving the well-known triple-deck structure. A systematic analysis of all the expansions and equations in the different layers has been carried out by the author (Roget, 1996) to determine the layer thicknesses and the gauge functions, depending on the values of the three parameters α, β and γ.

For $\alpha > \gamma$, $lz \gg lx$ and the flow is two-dimensional. For $\alpha < \gamma$, $lz \ll lx$ and the "corner-flow" problem is addressed. So fully three-dimensional problems are encountered only for $\alpha = \gamma$. Then, depending on the α and β values, four zones have been identified. Figure 2 shows the limits of these four zones depending on the hump's height (h) and horizontal size ($L = lx = lz$). The details of the demonstration can be found in Roget (1996). Zones 1 and 2 have linear equations in the lower deck, whereas zones 3 and 4, corresponding to higher protuberances, have non-linear ones. This frontier giving the critical height h_c had already been found for two-dimensional humps by Smith *et al.* (1981). Concerning the interaction, all four zones exhibit weak coupling properties, but in zones 1 and 3 the lower-deck equations are solved in direct mode with prescribed pressure, whereas in zones 2 and 4, corresponding to shorter humps, they are solved in inverse mode with prescribed displacement. To illustrate this, we will present the models corresponding to zones number 1 and 4.

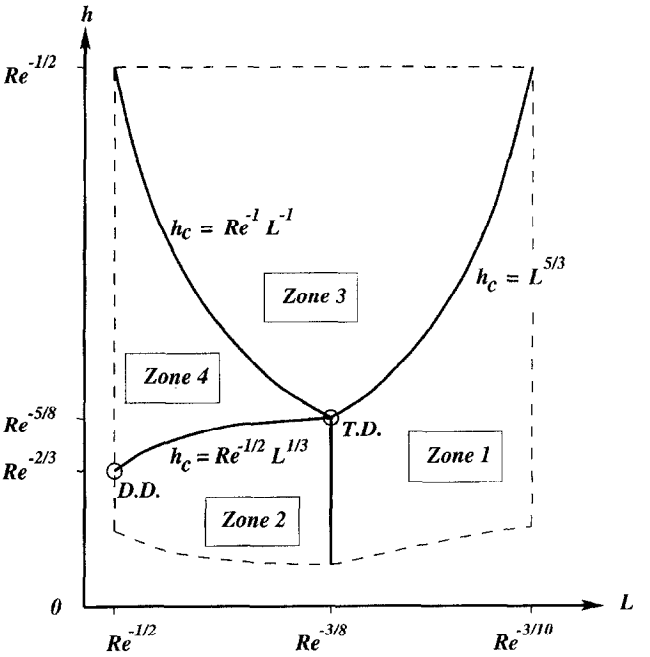

Fig. 2. – Delimitation of the four zones.

2.3. Model for zone 1

2.3.1. *Upper deck*

The normal variable in this deck is $Y^* = \dfrac{y}{\varepsilon^\alpha}$ and the expansions are :

$$(1) \qquad \begin{cases} u = 1 + \varepsilon^{\beta-\alpha}\, U_1^* + \cdots \\ v = \varepsilon^{\beta-\alpha}\, V_1^* + \cdots \\ w = \varepsilon^{\beta-\alpha}\, W_1^* + \cdots \\ p = \varepsilon^{\beta-\alpha}\, P_1^* + \cdots \end{cases}$$

All the perturbations have the same gauge. The first-order equations are just linearized Euler equations :

$$(2) \qquad \begin{cases} \dfrac{\partial U_1^*}{\partial X} + \dfrac{\partial V_1^*}{\partial Y^*} + \dfrac{\partial W_1^*}{\partial Z} = 0 \\ \dfrac{\partial U_1^*}{\partial X} = -\dfrac{\partial P_1^*}{\partial X} \\ \dfrac{\partial V_1^*}{\partial X} + \dfrac{\partial^2 f}{\partial X^2} = -\dfrac{\partial P_1^*}{\partial Y^*} \\ \dfrac{\partial W_1^*}{\partial X} = -\dfrac{\partial P_1^*}{\partial Z} \end{cases}$$

2.3.2. *Main deck*

The normal variable of this deck is $Y = \dfrac{y}{\varepsilon^{m/2}}$ and the expansions are :

$$(3) \qquad \begin{cases} u = U_0(Y) + \varepsilon^{\beta-4\alpha/3}\, \overline{U_1} + \cdots \\ v = \varepsilon^{\beta-7\alpha/3+m/2}\, \overline{V_1} + \cdots \\ w = \varepsilon^{\beta-\alpha}\, \overline{W_1} + \cdots \\ p = \varepsilon^{\beta-\alpha}\, \overline{P_1} + \cdots \end{cases}$$

It should be noticed that the $\overline{W_1}$ gauge is small compared to the $\overline{U_1}$ gauge. The perturbation in this layer is thus quasi two-dimensional. Analytical solutions can be found for the corresponding equations :

$$\overline{U_1} = A(X,Z)\,\frac{dU_0}{dY} \qquad \overline{V_1} = -\frac{\partial A(X,Z)}{\partial X}\,U_0 \qquad \overline{W_1} = \frac{1}{U_0}\,D(X,Z)$$

where $D(X,Z)$ is such that :

$$\frac{\partial D(X,Z)}{\partial X} = -\frac{\partial \overline{P_1}}{\partial Z}$$

2.3.3 *Lower deck*

In the viscous sub-layer, the normal variable is $\tilde{Y} = \dfrac{y}{\varepsilon^{\alpha/3+m/2}}$ and the expansions are :

$$(4)\qquad \begin{cases} u = \varepsilon^{\alpha/3}\lambda\tilde{Y} + \varepsilon^{1-4\alpha/3}\tilde{U}_1 + \cdots \\ v = \varepsilon^{m/2-2\alpha+1}\tilde{V}_1 + \cdots \\ w = \varepsilon^{1-4\alpha/3}\tilde{W}_1 + \cdots \\ p = \varepsilon^{1-\alpha}\tilde{P}_1 + \cdots \end{cases}$$

where $\lambda = \lim_{Y\to 0} \dfrac{U_0(Y)}{Y}$. In contrast to the main deck, both $\tilde{U}_1$ and $\tilde{W}_1$ now have the same gauges. The perturbation is thus fully three-dimensional. The equations are linear, due to the dominating position in the u expansion of the term $\lambda\tilde{Y}$ coming from the Blasius solution :

$$(5)\qquad \begin{cases} \dfrac{\partial\tilde{U}_1}{\partial X} + \dfrac{\partial\tilde{V}_1}{\partial\tilde{Y}} + \dfrac{\partial\tilde{W}_1}{\partial Z} = 0 \\ \lambda\tilde{Y}\dfrac{\partial\tilde{U}_1}{\partial X} + \lambda\tilde{V}_1 = -\dfrac{\partial\tilde{P}_1}{\partial X} + \dfrac{\partial^2\tilde{U}_1}{\partial\tilde{Y}^2} \\ \dfrac{\partial\tilde{P}_1}{\partial\tilde{Y}} = 0 \\ \lambda\tilde{Y}\dfrac{\partial\tilde{W}_1}{\partial X} = -\dfrac{\partial\tilde{P}_1}{\partial Z} + \dfrac{\partial^2\tilde{W}_1}{\partial\tilde{Y}^2} \end{cases}$$

2.3.4. *Matching*

Matching the different expansions gives the following relations :

$$(6)\qquad V_1^*(0) = 0 \qquad \lim_{\tilde{Y}\to\infty}\tilde{U}_1 = \lambda A(X,Z) \qquad \tilde{W}_1 \underset{\tilde{Y}\to\infty}{\sim} \frac{D(X,Z)}{\lambda\tilde{Y}}.$$

The upper-deck problem does not depend on the other layers. Using Fourier transforms, an expression giving the wall pressure solution of (2) can be obtained :

$$(7)\qquad P_1^*(X,0,Z) = \overline{P}_1 = \tilde{P}_1 = \frac{1}{2\pi}\oint\!\!\!\!\!\!C\oint\!\!\!\!\!\!C \frac{1}{\sqrt{(X-\xi)^2+(Z-\eta)^2}}\,\frac{\partial^2 f}{\partial\xi^2}\,d\xi\,d\eta.$$

In the above equation, the C means "Cauchy principal value". The lower-deck equations are then solved with prescribed pressure, giving the displacement $A(X,Z)$, which in turn determines the higher-order main-deck solution. The coupling is thus weak, and in direct mode.

2.4. Model for zone 4

2.4.1. *Upper deck*

The normal variable of this deck is again $Y^* = \dfrac{y}{\varepsilon^{\alpha}}$ but due to the degeneracy of the first-order perturbations, the expansions now read :

$$(8)\qquad \begin{cases} u = 1 + \varepsilon^{2\beta-m}\, U_2^* + \cdots \\ v = -\varepsilon^{\beta-\alpha}\dfrac{\partial f}{\partial X} + \varepsilon^{2\beta-m}\, V_2^* + \cdots \\ w = \varepsilon^{2\beta-m}\, W_2^* + \cdots \\ p = \varepsilon^{2\beta-m}\, P_2^* + \cdots \end{cases}$$

The first term in v expansion is only due to the Prandtl shift. The equations have lost the source term with f :

$$(9)\qquad \begin{cases} \dfrac{\partial U_2^*}{\partial X} + \dfrac{\partial V_2^*}{\partial Y^*} + \dfrac{\partial W_2^*}{\partial Z} = 0 \\ \dfrac{\partial U_2^*}{\partial X} = -\dfrac{\partial P_2^*}{\partial X} \\ \dfrac{\partial V_2^*}{\partial X} = -\dfrac{\partial P_2^*}{\partial Y^*} \\ \dfrac{\partial W_2^*}{\partial X} = -\dfrac{\partial P_2^*}{\partial Z} \end{cases}$$

2.4.2. *Main deck*

The normal variable of this deck is always $Y = \dfrac{y}{\varepsilon^{m/2}}$ and the expansions are :

$$(10)\qquad \begin{cases} u = U_0(Y) + \varepsilon^{\beta-m/2}\, f\dfrac{dU_0}{dY} + \varepsilon^{2\beta+\alpha-3m/2}\,\overline{U_2} + \cdots \\ v = -\varepsilon^{\beta-\alpha}\dfrac{\partial f}{\partial X}U_0 + \varepsilon^{2\beta-m}\,\overline{V_2} + \cdots \\ w = \varepsilon^{2\beta-m}\,\overline{W_2} + \cdots \\ p = \varepsilon^{2\beta-m}\,\overline{P_2} + \cdots \end{cases}$$

with the same expressions for $\overline{U_2}$, $\overline{V_2}$, and $\overline{W_2}$ that in zone 1 for $\overline{U_1}$, $\overline{V_1}$, and $\overline{W_1}$.

2.4.3. *Lower deck*

The normal variable for the lower deck is $\tilde{Y} = \dfrac{y}{\varepsilon^{(\alpha-\beta)/2+3m/4}}$ and the expansions are :

$$(11)\qquad \begin{cases} u = \varepsilon^{\beta-m/2}\tilde{U}_1 + \varepsilon^{(\alpha-\beta)/2+m/4}\lambda\tilde{Y} + \cdots \\ v = \varepsilon^{(\beta-\alpha)/2+m/4}\,\tilde{V}_1 + \cdots \\ w = \varepsilon^{\beta-m/2}\,\tilde{W}_1 + \cdots \\ p = \varepsilon^{2\beta-m}\,\tilde{P}_1 + \cdots \end{cases}$$

The inversion of the two terms in the u expansion leads to non-linear equations :

$$(12)\qquad \begin{cases} \dfrac{\partial \tilde{U}_1}{\partial X} + \dfrac{\partial \tilde{V}_1}{\partial \tilde{Y}} + \dfrac{\partial \tilde{W}_1}{\partial Z} = 0 \\ \tilde{U}_1 \dfrac{\partial \tilde{U}_1}{\partial X} + \tilde{V}_1 \dfrac{\partial \tilde{U}_1}{\partial \tilde{Y}} + \tilde{W}_1 \dfrac{\partial \tilde{U}_1}{\partial Z} = -\dfrac{\partial \tilde{P}_1}{\partial X} + \dfrac{\partial^2 \tilde{U}_1}{\partial \tilde{Y}^2} \\ \dfrac{\partial \tilde{P}_1}{\partial \tilde{Y}} = 0 \\ \tilde{U}_1 \dfrac{\partial \tilde{W}_1}{\partial X} + \tilde{V}_1 \dfrac{\partial \tilde{W}_1}{\partial \tilde{Y}} + \tilde{W}_1 \dfrac{\partial \tilde{W}_1}{\partial Z} = -\dfrac{\partial \tilde{P}_1}{\partial Z} + \dfrac{\partial^2 \tilde{W}_1}{\partial \tilde{Y}^2}. \end{cases}$$

2.4.4. *Matching*

Matching the different expansions gives the following relations :

$$(13)\qquad V_2^*(0) = -\frac{\partial A}{\partial X}(X,Z) \qquad \lim_{\tilde{Y}\to\infty} \tilde{U}_1 = \lambda f(X,Z) \qquad \tilde{W}_1 \underset{\tilde{Y}\to\infty}{\sim} \frac{D(X,Z)}{\lambda \tilde{Y}}.$$

The lower-deck problem must now be solved with a prescribed displacement, equal to f, to obtain the wall pressure. Then, given this pressure, the upper-deck provides the second-order displacement function A. The coupling is again weak, but now in inverse mode.

2.5. Discussion

The four zones thus correspond to different asymptotic structures. On the limit between linear and non-linear areas, both terms are retained since they have the same order of magnitude. On the limit between direct and inverse modes the strong coupling appears, where upper deck and lower deck depend on each other. The hierarchy is there broken.

In particular, the standard three-dimensional Triple-Deck model (Smith *et al.*, 1977; Bogolepov and Lipatov, 1985) is found for the values $\alpha = \gamma = 3m/8$ and $\beta = 5m/8$, exactly at the cross point of all four zones (label T.D. on Figure 2). That explains why it presents least degeneracy for non-linear terms, and strong coupling. The triple-deck model thus includes the properties of all four zones. On the opposite side, a special double-deck structure (label D.D. on Figure 2) appears, also on the linear/non-linear limit. It corresponds to the point where the upper-layer thickness becomes equal to the intermediate layer thickness. The hump is so small there that it does not disturb the inviscid flow. This structure is also encountered in pipe flows where there is no inviscid layer.

A weak coupling makes it possible to solve alternately a sequence of inviscid and boundary-layer problems in direct or inverse mode, depending on whether the pressure or displacement is known. On the other hand, the strong coupling requires both problems to be solved simultaneously, and an efficient numerical algorithm should closely respect this principle.

3. Interactive model

It can be shown that both lower-deck and main-deck equations are contained in Prandtl's three-dimensional boundary-layer equations, and the upper-deck equations are equivalent to the small perturbation form of the Euler equations. However, the usual matching conditions for the boundary layer with the wall pressure imposed

by the inviscid flow induce a weak coupling, and should thus be dropped. An alternative model for finite Reynolds number can be developed from the Triple Deck : by a simultaneous solving of the boundary-layer and inviscid equations together with the Triple-Deck interaction law, the strong interaction and the Triple-Deck structure can be taken into account (Veldman, 1979). This principle has been extended to three-dimensional boundary layers by Edwards (1987). The method used here is similar.

3.1. Boundary layer equations

The three-dimensional boundary-layer equations read :

$$\begin{cases} \dfrac{\partial u'}{\partial x'} + \dfrac{\partial V'}{\partial Y'} + \dfrac{\partial w'}{\partial z'} = 0 \\ u' \dfrac{\partial u'}{\partial x'} + V' \dfrac{\partial u'}{\partial Y'} + w' \dfrac{\partial u'}{\partial z'} = -\dfrac{\partial p}{\partial x'} + \dfrac{\partial^2 u'}{\partial Y'^2} \\ u' \dfrac{\partial w'}{\partial x'} + V' \dfrac{\partial w'}{\partial Y'} + w' \dfrac{\partial w'}{\partial z'} = -\dfrac{\partial p}{\partial z'} + \dfrac{\partial^2 w'}{\partial Y'^2} \\ \dfrac{\partial p}{\partial Y'} = 0 \end{cases} \tag{14}$$

The space coordinate and the velocity component normal to the wall Y' and V' are the usual boundary-layer stretched variables :

$$Y' = \sqrt{\mathrm{Re}}\, y' \qquad V' = \sqrt{\mathrm{Re}}\, v'.$$

With $F = \sqrt{\mathrm{Re}}\, \mathcal{F}$, the wall no-slip conditions are :

$$u' = 0 \qquad V' = 0 \qquad w' = 0 \qquad \text{for } Y' = F(x', z').$$

For convenience, a Prandtl shift is again applied to the boundary-layer equations. This allows us to write no-slip conditions at $Y = 0$ instead of $Y' = F(x, z)$. The new variables read :

$$\begin{cases} Y = Y' - F(x', z') & x = x' \qquad z = z' \\ V = V' - u' \dfrac{\partial F}{\partial x'} - w' \dfrac{\partial F}{\partial z'} & u = u' \qquad w = w' \end{cases}$$

The boundary-layer equations are left unchanged. Then, the normal velocity V is replaced by two stream functions ψ and ϕ defined as :

$$\frac{\partial \psi}{\partial Y} = u \qquad \frac{\partial \phi}{\partial Y} = w \qquad V = -\frac{\partial \psi}{\partial x} - \frac{\partial \phi}{\partial z}$$

The main advantages of these stream functions are to satisfy the continuity equation automatically and to match the integral displacement thicknesses (see below).

3.2. Inviscid flow and interaction law

The coupling is achieved by matching the normal velocities :

$$V_e(x', z') = \frac{V_\delta(x', z')}{\sqrt{\mathrm{Re}}} \quad \text{with} \quad V_\delta(x', z') = \lim_{Y' \to \infty} \left[V'(x', Y', z') + \left(\frac{\partial U_e}{\partial x'} + \frac{\partial W_e}{\partial z'} \right) Y' \right] \tag{15}$$

where U_e and W_e are the inviscid velocity components at the wall, and V_e is the blowing velocity at $y' = 0$ for the inviscid flow, representing both hump and boundary-layer displacement effects. After the Prandtl transformation, this equation reads :

$$V_\delta(x,z) = \lim_{Y\to\infty}\left[V(x,Y,z) + \left(\frac{\partial U_e}{\partial x} + \frac{\partial W_e}{\partial z}\right)Y + \frac{\partial F U_e}{\partial x} + \frac{\partial F W_e}{\partial z}\right]. \tag{16}$$

To prevent numerical oscillations in the boundary condition, it is preferable to use the integral thicknesses δ_1 and δ_2 defined as :

$$\delta_1 = \int_0^\infty \left(1 - \frac{u}{U_e}\right) dY \qquad \delta_2 = \int_0^\infty \frac{W_e - w}{U_e}\, dY$$

and (16) is replaced by :

$$V_\delta = \frac{\partial U_e\, \delta_1}{\partial x} + \frac{\partial U_e\, \delta_2}{\partial z} + \frac{\partial F U_e}{\partial x} + \frac{\partial F W_e}{\partial z}. \tag{17}$$

The first two terms of (17) represent the displacement due to the boundary layer, whereas the last two terms represent the hump's contribution.

The matching conditions for the stream functions are :

$$\lim_{Y\to\infty}[\psi - U_e Y] = -U_e\, \delta_1 \qquad \lim_{Y\to\infty}[\phi - W_e Y] = -U_e\, \delta_2.$$

To avoid loss of accuracy in ψ and ϕ due to $U_e Y$ when Y is large, the stream functions are changed into :

$$\overline{\psi} = \psi - U_e Y \qquad \overline{\phi} = \phi - W_e Y$$

The matching conditions thus become :

$$\lim_{Y\to\infty} \overline{\psi} = -U_e\, \delta_1 \qquad \lim_{Y\to\infty} \overline{\phi} = -U_e \delta_2. \tag{18}$$

U_e and W_e can be obtained from the Euler linearized equations with the wall condition taken from (15) and an approximation of (17), where U_e and W_e are replaced by U_{e0} and W_{e0} or by U_∞ and W_∞ in the integrands :

$$V_{BL} = \frac{\partial U_{e0}\, \delta_1}{\partial x} + \frac{\partial U_{e0}\, \delta_2}{\partial z} \qquad V_H = U_\infty \frac{\partial F}{\partial x} + W_\infty \frac{\partial F}{\partial z}$$

with :

$$U_{e0}(x,z) = U_\infty - \frac{1}{2\pi\sqrt{\mathrm{Re}}} \oint\!\!\oint \frac{1}{\sqrt{(x-\xi)^2 + (z-\eta)^2}} \frac{\partial V_H}{\partial \xi}\, d\xi\, d\eta \tag{19}$$

$$W_{e0}(x,z) = W_\infty - \frac{1}{2\pi\sqrt{\mathrm{Re}}} \oint\!\!\oint \frac{1}{\sqrt{(x-\xi)^2 + (z-\eta)^2}} \frac{\partial V_H}{\partial \eta}\, d\xi\, d\eta. \tag{20}$$

Then :

$$U_e(x,z) = U_{e0}(x,z) - \frac{1}{2\pi\sqrt{\mathrm{Re}}} \oint\!\!\oint \frac{1}{\sqrt{(x-\xi)^2 + (z-\eta)^2}} \frac{\partial V_{BL}}{\partial \xi}\, d\xi\, d\eta \tag{21}$$

$$W_e(x,z) = W_{e0}(x,z) - \frac{1}{2\pi\sqrt{\mathrm{Re}}} \oint\!\!\oint \frac{1}{\sqrt{(x-\xi)^2+(z-\eta)^2}} \frac{\partial V_{BL}}{\partial \eta}\, d\xi\, d\eta. \tag{22}$$

These equations are consistent with the coupling relation of the Triple-Deck theory if $U_\infty = 1$ and $W_\infty = 0$. U_{e0} and W_{e0} represent the inviscid velocity past the hump without the boundary layer. They are computed once at the beginning. Both integral relations (21) and (22) contain the elliptic nature of the problem, which requires an iterative solution.

3.3 Final form of the equations

In the boundary-layer equations, the pressure gradients are replaced by the foregoing expressions coming from Euler equations :

$$\frac{\partial p}{\partial x} = -U_e\frac{\partial U_e}{\partial x} - W_e\frac{\partial U_e}{\partial z} \qquad \frac{\partial p}{\partial z} = -U_e\frac{\partial W_e}{\partial x} - W_e\frac{\partial W_e}{\partial z}. \tag{23}$$

The normal coordinate is then changed into $\eta = \frac{Y}{H(x,z)}$ where $H(x,z)$ represents the computational domain height. The new boundary layer equations are :

$$\begin{cases} \dfrac{\partial \overline{\psi}}{\partial \eta} = H(u-U_e) \\ \dfrac{\partial \overline{\phi}}{\partial \eta} = H(w-W_e) \\ H\left(\dfrac{\partial \overline{\psi}}{\partial \eta} + HU_e\right)\dfrac{\partial u}{\partial x} - H\left[\dfrac{\partial}{\partial x}\left(\overline{\psi}+HU_e\eta\right) + \dfrac{\partial}{\partial z}\left(\overline{\phi}+HW_e\eta\right)\right]\dfrac{\partial u}{\partial \eta} \\ \qquad\qquad +H\left(\dfrac{\partial \overline{\phi}}{\partial \eta} + HW_e\right)\dfrac{\partial u}{\partial z} - H^2\left(U_e\dfrac{\partial U_e}{\partial x} + W_e\dfrac{\partial U_e}{\partial z}\right) - \dfrac{\partial^2 u}{\partial \eta^2} = 0 \\ H\left(\dfrac{\partial \overline{\psi}}{\partial \eta} + HU_e\right)\dfrac{\partial w}{\partial x} - H\left[\dfrac{\partial}{\partial x}\left(\overline{\psi}+HU_e\eta\right) + \dfrac{\partial}{\partial z}\left(\overline{\phi}+HW_e\eta\right)\right]\dfrac{\partial w}{\partial \eta} \\ \qquad\qquad +H\left(\dfrac{\partial \overline{\phi}}{\partial \eta} + HW_e\right)\dfrac{\partial w}{\partial z} - H^2\left(U_e\dfrac{\partial W_e}{\partial x} + W_e\dfrac{\partial W_e}{\partial z}\right) - \dfrac{\partial^2 w}{\partial \eta^2} = 0 \\ \dfrac{\partial p}{\partial Y} = 0 \end{cases} \tag{24}$$

with the boundary conditions :

$$\begin{cases} \eta = 0: & u = 0 & w = 0 & \overline{\psi} = 0 & \overline{\phi} = 0 \\ \eta = 1: & u = U_e & w = W_e & \overline{\psi} = -U_e\delta_1 & \overline{\phi} = -U_e\delta_2. \end{cases} \tag{25}$$

These equations are very close to those of Edwards (1987). We will no longer write the overlines on the stream functions in order to clarify the equations. The first two equations of (24) will be called "continuity" equations.

The principle of the present method is to solve the system of equations formed by (24), (21) and (22) simultaneously together with the boundary conditions (25).

4. Numerical method

The numerical method is similar to those used in previous works for this kind of problem. A few improvements have been made concerning the discretization of the Cauchy integrals and the boundary conditions.

4.1. Discretization of the boundary-layer equations

The numerical scheme is a second-order accurate finite-differencing in the x and y directions. The choice of a main direction for the flow is more complex than in a two-dimensional case since we know that w can be locally greater than u. However we decided to keep Ox as the principal direction of the flow since this will be true in the major part of the flow field.

The various derivative terms are obtained as follow :

• For the x-derivatives, we use a second-order backward scheme. This scheme has been kept everywhere, even in the small regions where reversed flow is encountered. No instabilities occurred even in such regions.

• The z-derivatives are calculated according to the direction of the local streamline. At each point of the mesh, the z-derivative scheme uses the previous point $(k-1)$ in the z-direction if $w \geq 0$ and the next point $(k+1)$ if $w < 0$. This means that it takes into account the characteristic direction of the local flow, and is similar to the scheme used in the 3-D boundary layer code $3C3D$ (Houdeville *et al.*, 1993). For an unknown function G, we write :

$$(26) \qquad \begin{cases} w\dfrac{\partial G}{\partial z} = w\,\alpha_1 \dfrac{G_k - G_{k-1}}{h_{z(k-1)}} + w\,\alpha_2 \dfrac{G_{k+1} - G_k}{h_{z(k)}} \\ \text{with :} \quad \alpha_1 = 1 \;\; \alpha_2 = 0 \quad \text{if } w \geq 0 \\ \text{or :} \quad\;\; \alpha_1 = 0 \;\; \alpha_2 = 1 \quad \text{if } w < 0 \end{cases}$$

where $h_{z(k-1)}$ is the step size in z direction and k is the node index along z.

• the y-derivatives have been discretized centered around η_j for the momentum equations, and around $\eta_{j-1/2}$ for the continuity equations. This difference is due to the fact that there are no second-order derivatives in the continuity equations.

The discretization of system (24) leads to a system of nonlinear equations written from the first point above the wall $j = 2$ to the point just before the upper boundary $j = m_y - 1$ for the momentum equations. The continuity equations are written from $j = 2$ to the upper boundary $j = m_y$.

4.2. Discretization of the interaction law

The two integral relations (21) and (22) have to be discretized. For convenience, we write :

$$A^1 = U_{e0}\,\delta_1 \qquad\qquad A^2 = U_{e0}\,\delta_2.$$

The discretization of these relations leads to :

$$U_{eik} = U_{e0ik} + \sum_{s=1}^{m_x}\sum_{t=1}^{m_z}(P^1_{st}A^1_{st} + P^2_{st}A^2_{st})$$

$$W_{eik} = W_{e0ik} + \sum_{s=1}^{m_x}\sum_{t=1}^{m_z}(P^3_{st}A^1_{st} + P^4_{st}A^2_{st})$$

where m_x and m_z are the number of grid points in the x and z directions, and P^1, P^2, P^3 and P^4 are functions of the mesh steps in the x and z directions, and of the gridpoint (i, k). For the iteration N, at the node (i, k), the semi-implicit scheme is defined as :

$$U^N_{eik} - P^{1N}_{ik}A^{1N}_{ik} - P^{2N}_{ik}A^{2N}_{ik} = R^{1N}_{ik} + R^{1N-1}_{ik}$$

$$W_{eik}^{N} - P_{ik}^{3N} A_{ik}^{1N} - P_{ik}^{4N} A_{ik}^{2N} = R_{ik}^{2N} + R_{ik}^{2N-1}$$

where the left-hand side terms are the unknowns,

R_{ik}^{1N} and R_{ik}^{2N} are all the terms of the sums already calculated at this iteration N,

R_{ik}^{1N-1} and R_{ik}^{2N-1} are terms not yet calculated but taken from the previous iteration.

4.3. Computational procedure

The method consists of a forward-marching technique in the x direction and then in the z direction. At each point of the (x,z) domain, the four unknowns U_e, W_e, δ_1 and δ_2 are determined *simultaneously*. Sweeping in x and z directions is repeated until convergence. The discretization leads to a set of nonlinear equations, which are solved with Newton's method. The Newton iteration will be called local iteration, whereas the iteration over all the x and z domain used to handle the ellipticity will be called global iteration.

All the variables u, w, ψ and ϕ in the boundary layer can be eliminated to end up with a system of four equations with only U_e, W_e, δ_1 and δ_2 as unknowns. Indeed, the discretization of (24) together with the Newton method gives a set of equations represented by a 4,4 block tridiagonal matrix with two additional columns due to U_e and W_e, which is inverted from the wall to the upper boundary $j = m_y$ using the boundary and matching conditions. This gives us a system of two equations with four unknowns. The last two relations which allow us to solve the entire system are given by (21) and (22). We have now 4 relations with 4 unknowns U_e, W_e, δ_1 and δ_2, from which the boundary layer profiles can be deduced.

Due to the second-order backward difference scheme, the values must be given for two z-grid lines upstream of the computed domain. To prevent spurious oscillations near the domain entry, the velocity perturbations U_e and W_e are linearly extrapolated and Blasius profiles matched with these inviscid velocities are imposed on these two grid lines. On the lateral faces, the z-derivatives are taken towards the domain center. Thereby, the perturbation is not forced to zero on the domain faces.

5. Results

The quasi-simultaneous method has been used to compute high Reynolds number flows past a flat plate with various three-dimensional obstacles in order to investigate the flow structure near separation. The results for three different shapes will be presented here and compared with other results available in the literature.

The general obstacle shape is given by the equation :

$$y = f(x,z) = h \ \mathrm{sech}\Big(4(x-2.5)\Big)\mathrm{sech}\Big(4z\Big)$$

The center of the protuberance is located at $L_0 = 2.5$ from the leading-edge. This shape has been previously calculated by several authors (Smith, 1991; Edwards, 1987; Davis *et al.*, 1989). Edwards' results are obtained using the quasi-simultaneous method. Those from Davis are solutions of the Navier-Stokes equations in vorticity-stream-function formulation. Smith uses a three-dimensional interacting boundary-layer in skewed shears formulation, with linear quasi-planar sweeps of the boundary layer. The comparative plots are taken from Davis *et al.* (1989), including the results of Edwards (1987).

5.1. 3% THREE-DIMENSIONAL TROUGH

The first protuberance is a trough ($h = -0.03$). A calculation with an upstream reference Reynolds number of 80 000 has been performed using a 71×71 mesh on the surface $(x, z) = [1, 5] \times [-1.5, +1.5]$. The grid had 91 points between $y = 0$ and $y = \dfrac{30}{\sqrt{\mathrm{Re}}}$.

A comparison of the axial skin friction distribution at three different z stations (symmetry line, z=0.3 and z=0.6) is shown in Figure 3. This figure points out that the results given by the three methods are in very good agreement. The positive axial pressure gradient causes the axial skin friction to decrease, giving rise to a reversed flow region (negative C_{fx}). On the symmetry line, the separation occurs about $x = 2.25$, and the reattachment takes place around $x = 2.6$. The spanwise skin friction distributions are plotted in Figure 4 for the same z stations, except z=0 which is the symmetry line (w=0). The results are still in very good agreement, even if minor differences are seen near the symmetry line. No visible oscillations occur on the simultaneous solution near the domain entry, thanks to the regularity of the boundary condition.

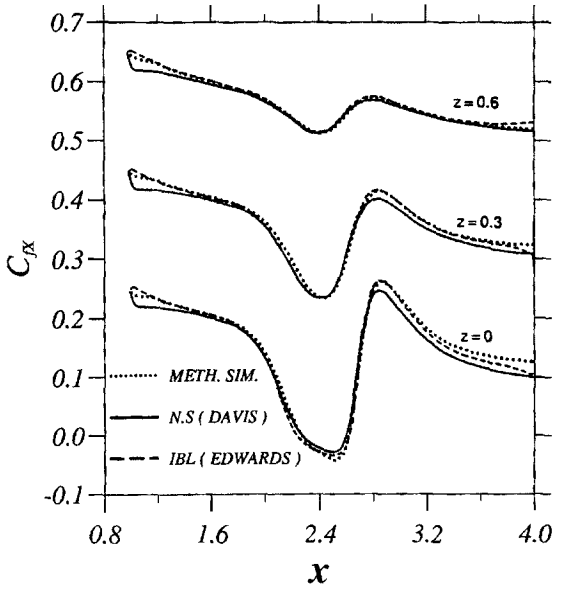

Fig. 3. - Axial component of skin friction - 3 % 3-D trough.

5.2. 2.7% THREE-DIMENSIONAL TROUGH

The second case is a slightly different trough, now with $h = -0.027$. The Reynolds number is again 80 000 and the same mesh as before was used. The grid influence has been checked by Roget (1996) : the results obtained with 71×71 or 91×91 grids in the (x, z) plane are quasi identical.

Figure 5 shows the skin friction lines for this case. The flow pattern is very similar to the Figure 4 of Edwards (1987), obtained with IBL, and the Figure 4 of Davis *et al.* (1989) obtained with Navier-Stokes solution. The validity of the boundary-layer equations for this kind of problem is thus confirmed. The very good symmetry of the result with no artificial symmetry condition imposed can be noticed. The unsymmetrical z-sweeping has thus no influence. Two singular points are present in this figure :

- the saddle point of separation (Delery, 1990, 1992; Peake and Tobak, 1982), which is represented in Figure 6.
- the reattachment node, which is represented in Figure 7.

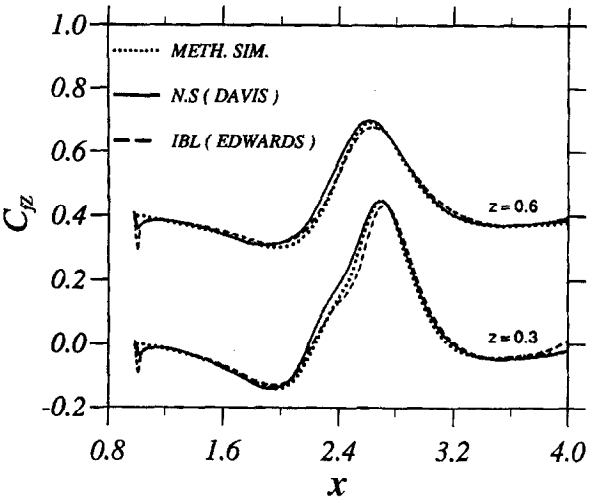

Fig. 4. – Spanwise component of skin friction - 3 % 3-D trough.

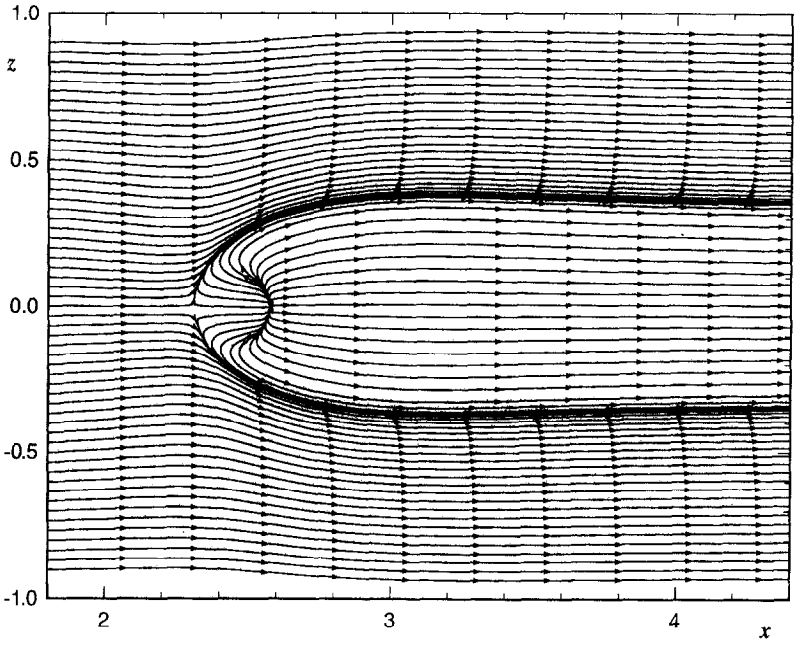

Fig. 5. – Skin friction lines - 2.7 % 3-D trough.

Figure 5 also shows the "corridor" effect produced by separation on the friction lines topology. No streamline coming from upstream can penetrate inside this corridor, while all streamlines inside come from the same point, the reattachment point. The frontier is constituted by the separation line, going through the saddle point, and along which occurs a congregation of the neighbouring streamlines. This "corridor" effect was predicted by previous triple-deck studies (Smith *et al.*, 1977).

In order to help topological understanding of three-dimensional separation, we study the velocity projections in planes xy or zy normal to the wall. It is interesting to draw the *pseudo-streamlines* of this projected velocity. Except in the symmetry plane, these pseudo-streamlines are not real streamlines. Nevertheless, this technique

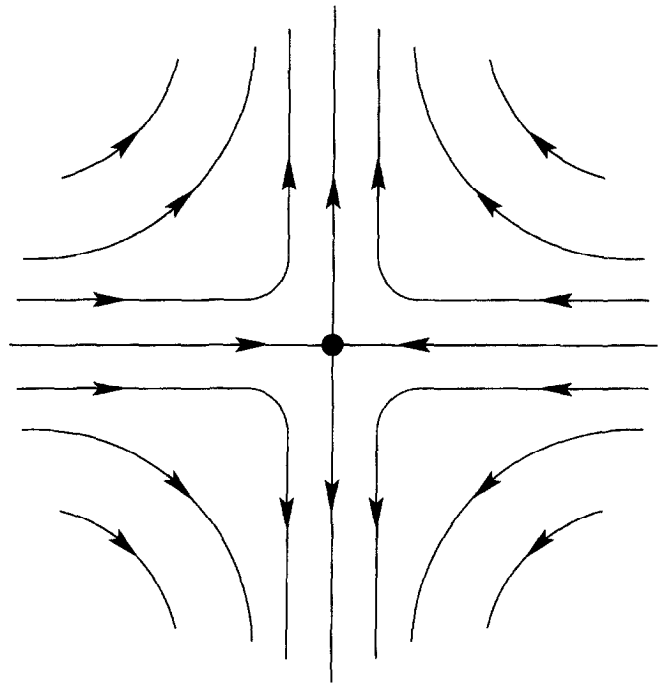

Fig. 6. – Schematic view of a saddle-point.

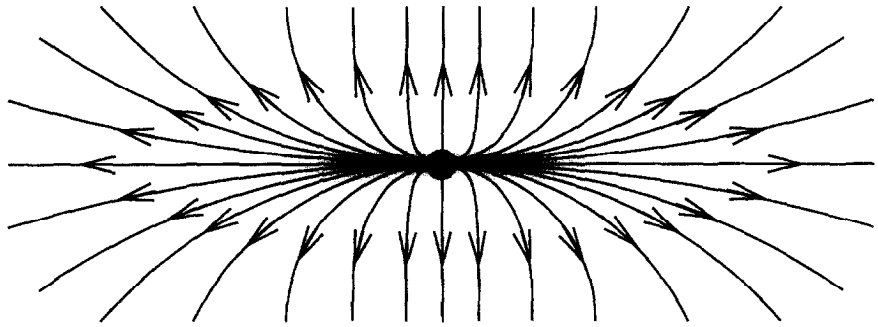

Fig. 7. – Schematic view of a node.

provides an appreciable help to understand complex three-dimensional flows when the analysis of the skin friction lines is not sufficient.

The pseudo-streamlines drawn with the (u, v) velocity components in the plane $z = 0.043$, close to the symmetry plane, are shown in Figure 8. A vortex structure obviously appears. Three particular features can be pointed out in this figure. First, a stable focus which is the core of the vortex. This focus stands just before the centre of the trough ($x = 2.5$). Second, a separation line (label 2 in the figure) upstream of the vortex: this line goes from the wall to the vortex core. The last feature is another separation line (label 1 in the figure): this line separates the pseudo-streamlines which go inside the vortex from those going downstream. The former are ejected normally to the (x, y) plane.

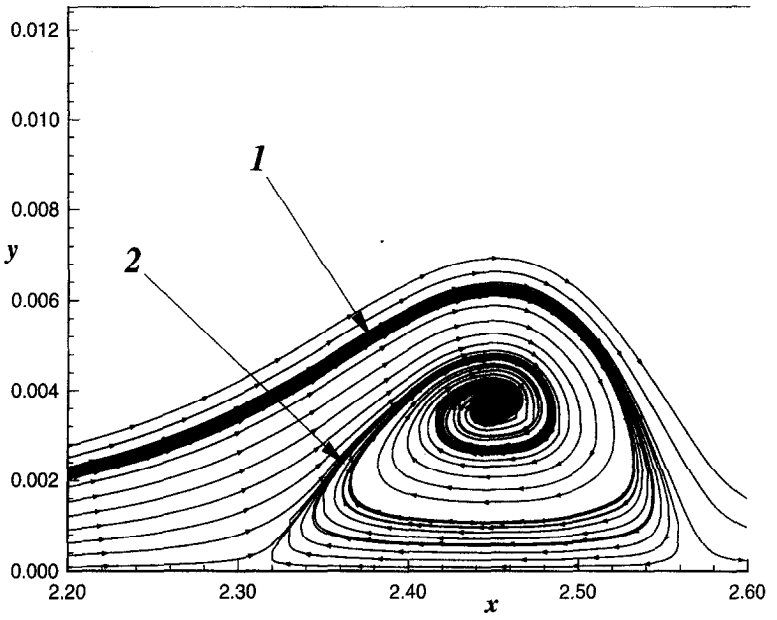

Fig. 8. – Pseudo-streamlines in the plane $z = 0.043 - 2.7\ \%$ 3-D trough.

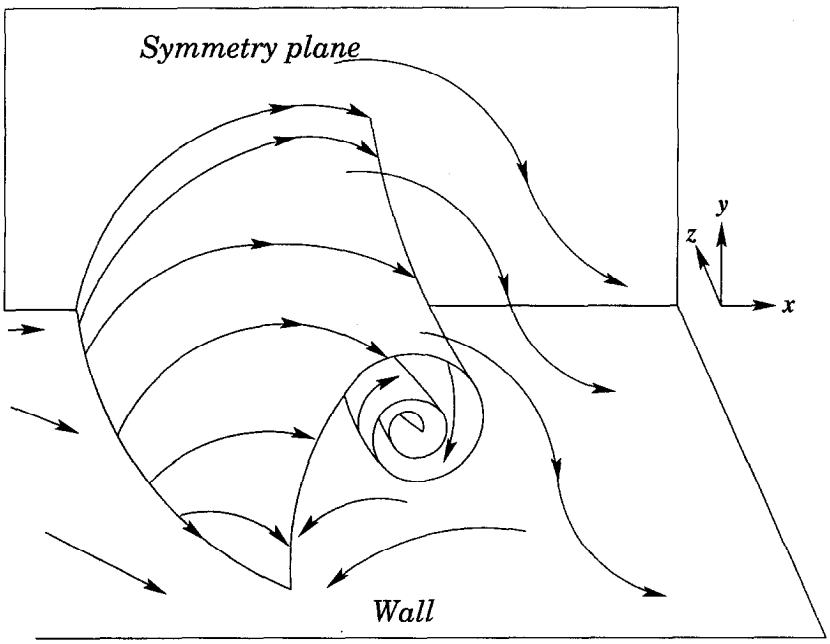

Fig. 9. – Schematic view of a horse-shoe vortex.

According to Figures 5 and 8, the flow structure can be identified as a horse-shoe vortex (Delery, 1990, 1992). The horse-shoe vortex structure is schematically represented in Figure 9. All the streamlines coming from upstream are rejected on the side of the horse-shoe vortex (see Tobak and Peake, 1982; Legendre, 1977; Yates, 1992). Figure 10 represents the trajectory of a particle coming into the vortex. After several turns, it is ejected on the side. This scheme explains Figure 11 on which are plotted some three-dimensional streamlines.

The horse-shoe vortex is fed by oncoming streamlines close to the wall and close to the symmetry plane. The streamlines coming from the higher part of the upstream boundary layer are seen to cross over the vortex with a small transverse deviation. This agrees with the two-dimensional-like equations obtained for the main-deck in the asymptotic analysis.

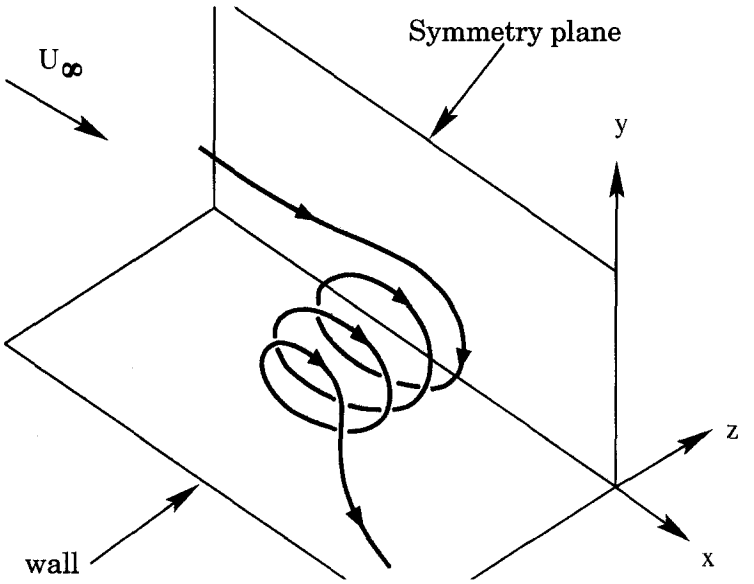

Fig. 10. – Schematic three-dimensional streamlines - 2.7 % 3-D trough.

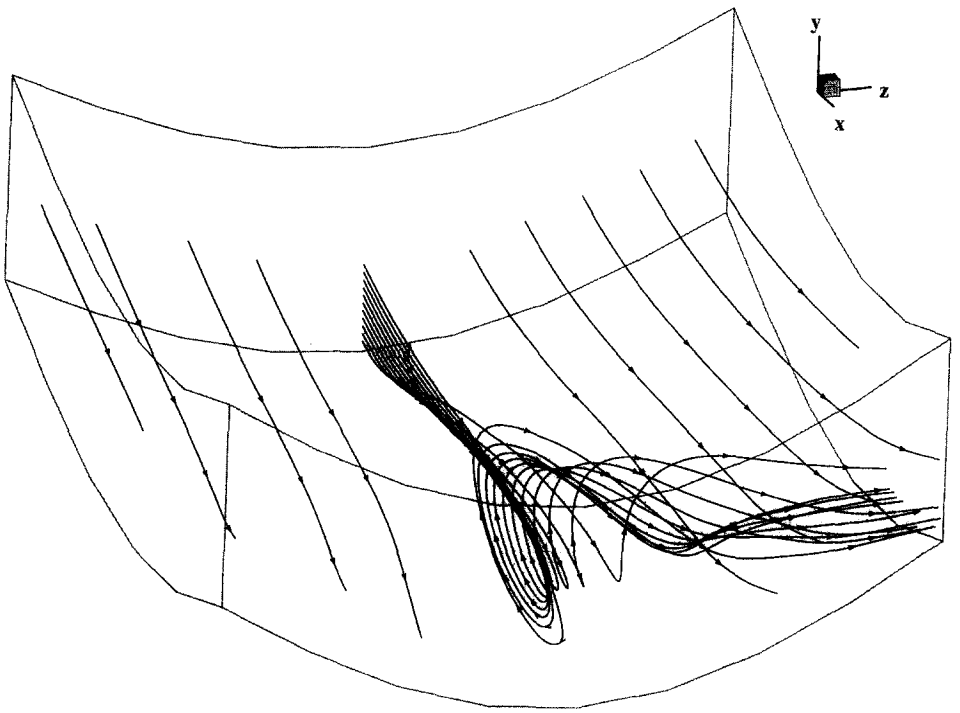

Fig. 11. – Three-dimensional streamlines - 2.7 % 3-D trough.

5.3. 3% THREE-DIMENSIONAL HUMP

The results for this case also come from the papers of Edwards (1987) and Davis *et al.* (1989). The upstream reference Reynolds number is now 60 000 and the same mesh has been used as in both previous cases.

The limiting streamlines, or skin friction lines, are plotted in Figure 12. This picture is again similar to those of Edwards (1987) and Davis *et al.* (1989). This figure brings into evidence a strong difference in the topological layout of the flow between the hump and the trough. The only common feature is that there are two singular points on the symmetry line. At the separation point on the symmetry line lies a node called "stable" (Delery, 1992), since all the skin friction lines converge towards the singular point. The second singular point is found downstream on the symmetry line and is a saddle-point. The "corridor" is now upstream of the hump.

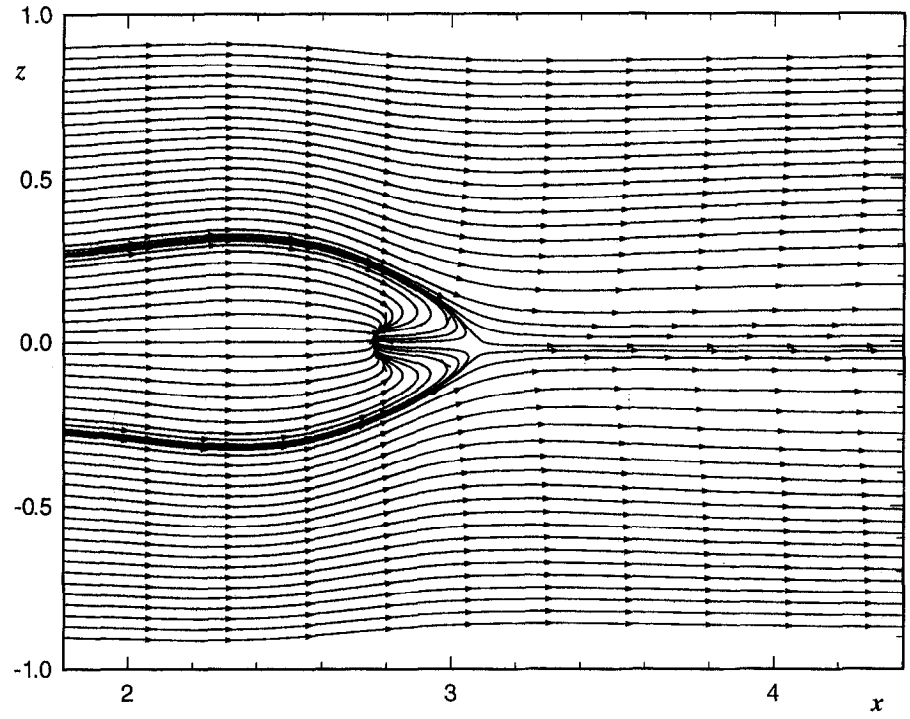

Fig. 12. – Skin friction lines - 3 % 3-D hump.

The strong difference between the hump and the trough is the result of the spanwise velocity. When separation occurs, the spanwise velocity effect is the opposite of that seen in the case of the trough. All the skin friction lines are driven towards the symmetry plane. The skin friction lines topology for the hump is close to that observed on a hemisphere-cylinder at small incidence (1°) (Peake and Tobak, 1982) whereas the trough has the horse-shoe vortex topology.

Figure 13 shows the pseudo-streamlines plotted with the velocity (u, v) in the plane z=0.043. For this plot, the Prandtl shift has not been reversed. This figure shows a separation line (1) upstream of the reversed region. All the streamlines coming from upstream bypass the reversed region. All the streamlines inside come from a nodal point called the "focus". This focus represents the physical axis around which the streamlines turn. A

second separation line (2) limits the reversed region downstream. It can be also noticed that there is no closed bubble as in two-dimensional separations, except in the symmetry plane. Figure 14 shows schematically the "S" shape of the three-dimensional streamlines, which are plotted in Figure 15. No vortex structure can be seen on this picture, but one can see that the reversed region is fed by streamlines coming from the sides of the hump.

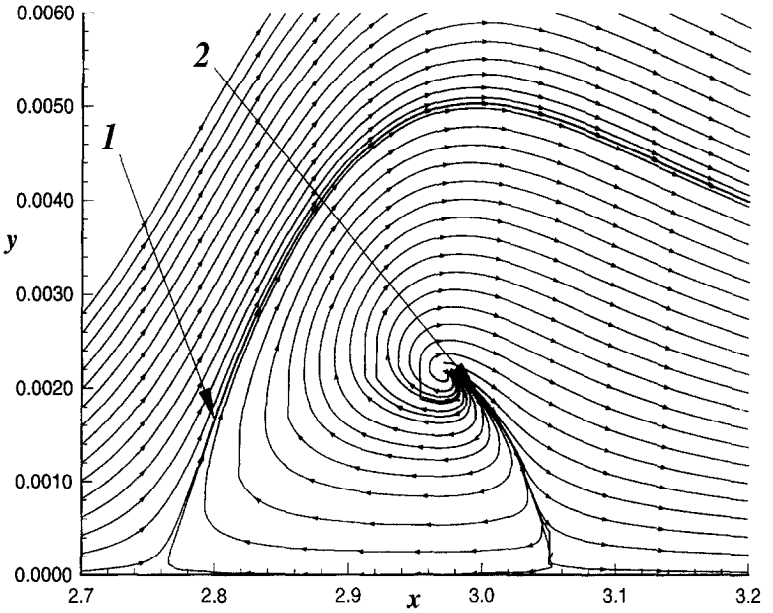

Fig. 13. – Pseudo-streamlines in the plane $z = 0.043$ - 3 % 3-D hump.

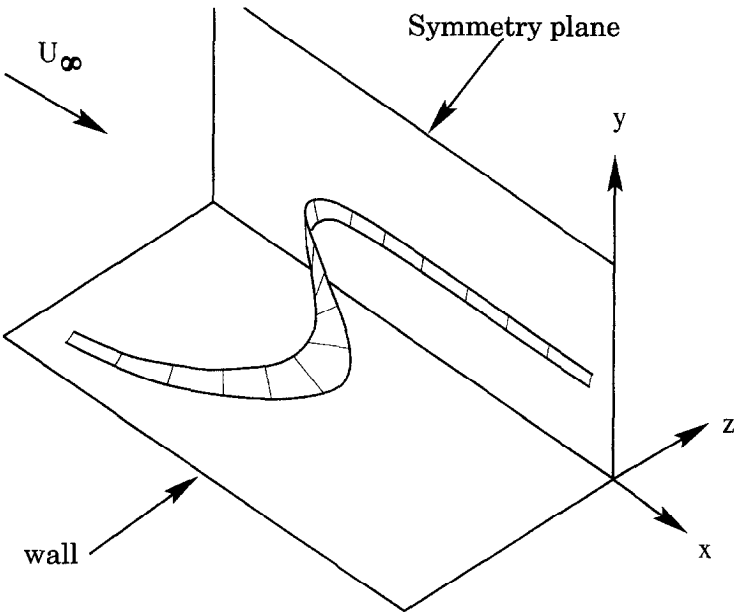

Fig. 14. – Schematic three-dimensional streamlines - 3 % 3-D hump.

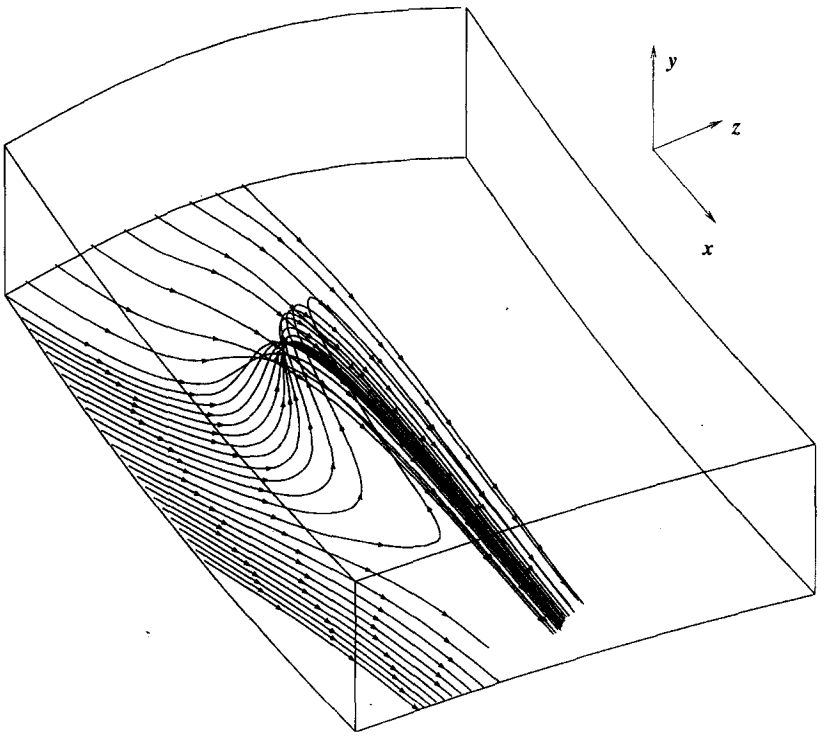

Fig. 15. – Three-dimensional streamlines - 3 % 3-D hump.

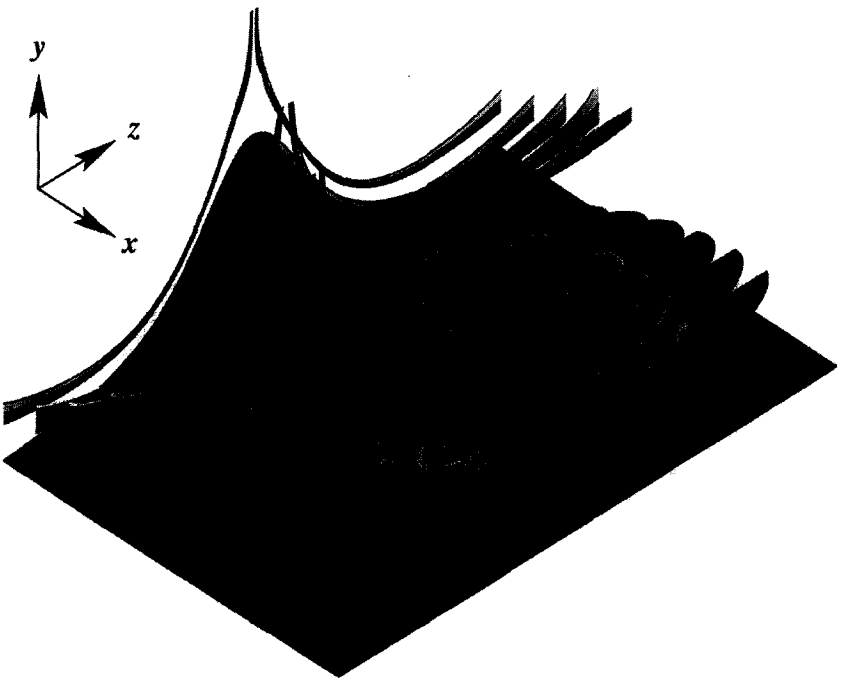

Fig. 16. – Helicity density contours - 3 % 3-D hump.

The helicity density (Levy *et al.*, 1990) is plotted in Figure 16. This helicity density is defined by :

$$H_d = \vec{U}.\vec{\omega}$$

where $\vec{U}$ is the velocity and $\vec{\omega}$ is the vorticity. This helicity density is a useful variable to put into evidence the rotating regions. In this way, looking at Figure 16, two symmetrical vortices with longitudinal axis obviously appear downstream of the hump. They turn in opposite directions.

6. Conclusion

A systematic asymptotic analysis has been performed for a boundary layer encountering a three-dimensional protuberance. Depending on the obstacles asymptotic dimensions, four different structures surrounding the well-known triple-deck have been brought into evidence. These four structures are degenerated forms of the triple-deck model, but they illuminate its properties, such as the fusion of both weak coupling direct and inverse modes towards strong interaction.

Using the interacting boundary-layer method, grounded on asymptotic considerations, it has been possible to study the complex topology of the three-dimensional flow near separation. In particular, the skin friction diagrams, the pseudo-streamlines in various planes normal to the wall, and the three-dimensional streamlines have been analyzed.

For the cases considered, some differences were found between the flow over a hump and in a trough. For the trough, a "horse-shoe vortex" structure has been demonstrated. On the other hand, for the hump, the reversed flow region is smaller in the spanwise direction and there is no "quasi two-dimensional bubble". In turn, the presence of the hump creates two axial vortices downstream of the hump. This leads to the conclusion that the structure of the reversed flow region is driven by the spanwise velocity.

Of course, these results should be confirmed by several other computations or experiments to determine possible bifurcations in the flow structure when the Reynolds number or the obstacle's shape or dimensions are modified. Nevertheless, the quasi-simultaneous method constitutes a powerful tool to explore the physical structure of the flow for various three-dimensional obstacles.

REFERENCES

BOGOLEPOV V. V., LIPATOV I. I., 1985, Locally three-dimensional laminar flow, *Journal Prikladnoi Mekhaniki i Tekhnicheskoi Fiziki*, **1**, 28-36.

DAVIS R. L., CARTER J. E., HAFEZ M., 1989, Three-dimensional viscous flow solutions with a vorticity-stream function formulation, *AIAA J.*, **27**, 892-900.

DELERY J., 1990, Physique des écoulements tourbillonnaires, in *Vortex Flow Aerodynamics*, pp. 20.1-20.32, AGARD, NATO.

DELERY J., 1992, Physics of vortical flows, *J. Aircraft*, **29**, 856-876.

DUCK P. W., BURGGRAF O. R., 1986, Spectral solutions for three-dimensional triple-deck flow over surface topography, *J. Fluid Mech.*, **162**, 1-22.

EDWARDS D. E., 1987, Analysis of 3-D separated flow using interacting boundary-layer theory, in *Proc. IUTAM Symposium on Boundary-Layer Separation*, ed. F.T. Smith and S. Brown, pp. 163-178, Springer-Verlag.

EDWARDS D. E., CARTER J. E., SMITH F. T., 1987, Analysis of the three-dimensional separated flow with the boundary-layer equations, *AIAA J.*, **25**, 380-387.

HOUDEVILLE R., MAZIN C., CORJON A., 1993, Méthode de caractéristiques pour le calcul de couches limites tridimensionnelles, *La Rech. Aérosp.*, **1977-6**, 37-49.

LE BALLEUR J. C., GIRODROUX-LAVIGNE P., 1992, Calculation of fully three-dimensional separated flows with an unsteady viscous-inviscid interaction method, 5^{th} *Int. Symp. on Numerical and Physical Aspects of Aerodynamic Flows*, T. Cebeci ed., California State University, Long Beach.

LEGENDRE R., 1977, Lignes de courant d'un écoulement permanent - Décollement et séparation, *La Rech. Aérosp.*, **6**, 327-335.

LEVY Y., DEGANI D., SEGINER A., 1990, Graphical visualization of vortical flows by means of helicity, *AIAA J.*, **28**, 1347-1352.

McDONALD H., BRILEY W. R., 1983, A survey of recent work on interacted boundary layer theory for flow with separation, *2nd Int. Symp. on Numerical and Physical Aspects of Aerodynamic Flows*, T. Cebeci ed., California State University, Long Beach.

MAUSS J., 1995, Asymptotic Modeling for separating boundary layers, in *Lectures Notes in Physics*, **442**, Springer Verlag.

PEAKE D. J., TOBAK M., 1982, Three-dimensional flows about simple components at angle of attack, *AGARD Lecture Series 121*, NATO.

RAGAB S. A., NAYFEH A. H., 1981, A comparison of the second-order triple-deck theory with interacting boundary layers, *Int. Symp. on Numerical and Physical Aspects of Aerodynamic Flows*, T. Cebeci ed., California State University, Long Beach.

ROGET C., BRAZIER J. Ph., MAUSS J., 1994, *Caractérisation à l'aide de structures en triple couche de l'influence d'une perturbation pariétale sur une couche limite bidimensionnelle*, Tech. Rep. DERAT 55/5604.61, ONERA-CERT, Toulouse, France.

ROGET C., 1996, *Structures asymptotiques et calculs d'écoulements sur des obstacles bi et tridimensionnels*, PhD thesis, Université Paul Sabatier, Toulouse, France.

ROTHMAYER A. P., BARNETT M., 1991, Constructing physics-based numerical schemes for viscous-inviscid interactions, *Comp. and Fluids*, **20**, No. 3, 201-211.

SMITH F. T., 1973, Laminar flow over a small hump on a flat plate, *J. Fluid Mech.*, **57**, part 4, 803-824.

SMITH F. T., 1976a, Pipeflows distorted by nonsymmetric indentation or branching, *Mathematika*, **23**, 62.

SMITH F. T., 1976b, On entry-flow effects in bifurcating, blocked or constricted tubes, *J. Fluid Mech.*, **78**, part 4, 709-736.

SMITH F. T., SYKES R. I., BRIGHTON P. W. M., 1977, A two–dimensional boundary layer encountering a three–dimensional hump, *J. Fluid Mech.*, **83**, part 1, 163-176.

SMITH F. T., 1980, A three-dimensional boundary-layer separation, *J. Fluid Mech.*, **99**, part 1, 185-224.

SMITH F. T., BRIGHTON P. W. M., JACKSON P. S., HUNT J. C. R., 1981, On boundary-layer flow past two-dimensional obstacles, *J. Fluid Mech.*, **113**, 123-152.

SMITH F. T., 1983, *Properties, and a finite-difference approach, for three-dimensional interacting boundary layers*, United Technologies UTRC Report UT 83-46.

SMITH F. T., 1986, Steady and unsteady boundary-layer separation, *Ann. Rev. Fluid Mech.*, **18**, 197-220.

SMITH F. T., 1991, Steady and unsteady 3D interactive boundary-layers, *Comp. and Fluids*, **20**, No. 3, 243-268.

STEWARTSON K., 1969, On the flow near the trailing edge of a flat plate II, *Mathematika*, **16**, 106-121.

SYKES R. J., 1980, On three-dimensional boundary layer flow over surface irregularities, *Proc. Roy. Soc. London A*, **373**, 311-329.

TOBAK M., PEAKE D. J., 1982, Topology of three-dimensional separated flows, *Ann. Rev. Fluid Mech.*, **14**, 61-85.

VELDMAN A. E. P., 1979, *A numerical method for the calculation of laminar, incompressible boundary layers with strong viscous–inviscid interaction*, Tech. Rep. 79023 U, NLR, The Netherlands.

VELDMAN A. E. P., 1981, New, quasi–simultaneous method to calculate interacting boundary layers, *AIAA J.*, **19**, 79-85.

HENKES R. A. W. M., VELDMAN A. E. P., 1987, On the breakdown of the steady and unsteady interacting boundary-layer description, *J. Fluid Mech.*, **179**, 513-529.

YATES L. A., CHAPMAN G. T., 1992, Streamlines, vorticity lines, and vortices around three-dimensional bodies, *AIAA J.*, **30**, 1819-1826

(Manuscript received March 19, 1997;
revised January 12, 1998;
accepted February 27, 1998.)